Title: Lunar basalt chronology, mantle differentiation and implications for determining the age of the Moon

Authors: Joshua F. Snape[1]*, Alexander A. Nemchin[1,2], Jeremy J. Bellucci[1], Martin J. Whitehouse[1,3], Romain Tartèse[4,5], Jessica J. Barnes[5], Mahesh Anand[5,6], Ian A. Crawford[7], Katherine H. Joy[8]

Affiliations:

[1] Department of Geosciences, Swedish Museum of Natural History, SE-104 05 Stockholm, Sweden.

[2] Department of Applied Geology, Curtin University, Perth, WA 6845, Australia.

[3] Department of Geological Sciences, Stockholm University, SE-106 91 Stockholm, Sweden.

[4] Institut de Minéralogie, de Physique des Matériaux et de Cosmochimie, Muséum National d'Histoire Naturelle, Sorbonne Universités, CNRS, UPMC & IRD, 75005 Paris, France.

[5] Planetary and Space Sciences, The Open University, Walton Hall, Milton Keynes MK7 6AA, UK.

[6] Department of Earth Sciences, The Natural History Museum, Cromwell Road, London, SW7 5BD, UK.

[7] Department of Earth and Planetary Sciences, Birkbeck College, University of London, Malet Street, London WC1E 7HX, UK.

[8] School of Earth, Atmospheric and Environmental Sciences, University of Manchester, Oxford Road, Manchester M13 9PL, UK.

*Corresponding author (joshua.snape@nrm.se)

Abstract

Despite more than 40 years of studying Apollo samples, the age and early evolution of the Moon remain contentious. Following the formation of the Moon in the aftermath of a giant impact, the resulting Lunar Magma Ocean (LMO) is predicted to have generated major geochemically distinct silicate reservoirs, including the sources of lunar basalts. Samples of these basalts, therefore, provide a unique opportunity to characterize these reservoirs. However, the precise timing and extent of geochemical fractionation is poorly constrained, not least due to the difficulty in determining accurate ages and initial Pb isotopic compositions of lunar basalts. Application of an *in situ* ion microprobe approach to Pb isotope analysis has allowed us to obtain precise crystallization ages from six lunar basalts, typically with an uncertainty of about ±10 Ma, as well as constrain their initial Pb-isotopic compositions. This has enabled construction of a two-stage model for the Pb-isotopic evolution of lunar silicate reservoirs, which necessitates the prolonged existence of high-μ reservoirs in order to explain the very radiogenic compositions of the samples. Further, once firm constraints on U and Pb partitioning behaviour are established, this model has the potential to help distinguish between conflicting estimates for the age of the Moon. Nonetheless, we are able to constrain the timing of a lunar mantle reservoir differentiation event at 4376±18 Ma, which is consistent with that derived from the Sm-Nd and Lu-Hf isotopic systems, and is interpreted as an average estimate of the time at which the high-μ urKREEP reservoir was established and the Ferroan Anorthosite (FAN) suite was formed.

Keywords

Lunar basalts; Pb isotopes; volcanism; lunar magma ocean; lunar origin

1. **Introduction**

The lunar magma ocean (LMO) model, proposed after the first analyses of the Apollo samples, remains the canonically accepted explanation for the magmatic differentiation of the Moon (Wood et al. 1970; Elkins-Tanton et al. 2011). In its current form, the model predicts the formation of a global magma ocean as a consequence of a Moon-forming "giant impact" between the Earth and a Mars-sized body (Hartmann and Davis 1975) ~60 million years (Ma) after Solar System formation at 4567 Ma (Touboul et al. 2007; Connelly et al. 2012; Avice and Marty 2014). Development of the major lunar rock suites then occurred as a result of cooling and differentiation of this magma ocean, followed by partial melting of the mantle reservoirs that formed during differentiation. However, the age of the LMO (and the Moon), as well as the time interval required for its crystallization, remain unclear. While W-isotope data, suggesting that the short-lived ^{182}Hf was extinct by the time of lunar formation (Touboul et al. 2007), place the oldest limit for the age of the LMO at about 4500 Ma, the attempts to define the youngest limit are based on studies of the oldest identified lunar rocks, represented by the highland samples. These samples are interpreted as remnants of either the primary anorthositic crust (Ferroan Anorthosites; FAN) that formed as part of the LMO differentiation sequence, or early plutonic magmatic rocks (Magnesian- and Alkali-Suite rocks; Elkins-Tanton et al. 2011; Carlson et al. 2014; Borg et al. 2015; Pernet-Fisher and Joy 2016). Crystallization age estimates for FANs range from 4290-4570 Ma, while the Magnesian-suite rocks have crystallization ages of 4110-4570 Ma, but analytical uncertainties for a significant number of these dates are often close to 100 million years or more (Borg et al. 2015). Such large uncertainties, and the wide range of overlapping ages for FAN and Magnesian-suite rocks, have led to the traditional LMO model for lunar differentiation being challenged in recent studies (Borg et al. 2011; Carlson et al. 2014; McLeod et al. 2014; Gaffney and Borg 2014). In particular, some of these studies suggested that the age of the Moon and the LMO may be more than 100 million years younger (i.e. ~4400 Ma) than indicated by other isotopic constraints (e.g. Avice and Marty 2014). The younger age of the Moon, however, conflicts with dates as old as 4417±6 Ma determined in zircon grains identified in lunar breccias, which have been interpreted as placing a lower time limit on the final stages of LMO crystallization (Nemchin et al. 2009).

The Apollo mare basalts have younger crystallization ages, typically between 3800-3000 Ma (e.g. Albee et al. 1970; Turner 1970; Papanastassiou et al. 1970; Davis et al. 1971; Murthy et al. 1971; Papanastassiou and Wasserburg 1971; Compston et al. 1971;1972; Nyquist et al. 1975;1979;1981; Guggisberg et a. 1979; Tartèse et al. 2013). Nevertheless, the melts from which these rocks crystallized are thought to have been sourced from silicate reservoirs in the lunar mantle generated during the LMO crystallization, therefore providing a link to this initial phase of the Moon's evolution. As such, four mare basalt and two KREEP-rich (material enriched in K, REE and P; Warren and Wasson 1979) basalt samples have been investigated using high spatial resolution Secondary Ion Mass Spectrometry (SIMS) to obtain a new set of Pb isotope data and help constrain early lunar magmatic evolution.

Previous attempts to apply Pb isotope systematics to fundamental questions related to the early history of the Moon have utilized Thermal Ionization Mass Spectrometry (TIMS) analyses of chemically separated Pb fractions. While this approach has been successfully applied to the investigation of differentiation processes on the Earth (e.g. Zartman and Doe 1981; Kramers and Tolstikhin 1997), the inherently low Pb concentrations in lunar samples (relative to those from the Earth) renders the data particularly susceptible to the influence of laboratory contamination. The low Pb content in lunar samples is thought to be a consequence of extensive loss of volatile Pb early in the history of the Moon (e.g. Tatsumoto 1970), most likely resulting from the giant Moon-forming impact. This concept is consistent with previous attempts to measure Pb isotopes in lunar samples (Tatsumoto 1970; Tera and Wasserburg 1972; Tatsumoto et al. 1987; Gaffney et al. 2007a; Nemchin et al. 2011), which indicate that the ratio of $^{238}U/^{204}Pb$ (μ) in many lunar rocks is significantly higher (~100-600) than μ-values inferred for the Earth's mantle (typically ~8-10; Zartman and Doe 1981; Kramers and Tolstikhin 1997). These high μ-values of lunar rocks also result in very radiogenic Pb isotope compositions, making it difficult to distinguish between analyses representing Pb accumulated in the samples by *in situ* radioactive decay of U (radiogenic Pb) and those reflecting the initial Pb composition inherited during crystallization, or various mixtures of the two. The high spatial resolution SIMS approach undertaken here makes it possible to limit contamination, focus on the

individual phases in which Pb is concentrated, and overcome the issues associated with the multi component Pb mixtures present in lunar samples, helping to determine both the crystallization ages of these samples and their initial Pb compositions.

2. Analytical Methods

2.1. Data acquisition

Four of the samples (10044,645; 12039,44; 14072,61 and 15386,46) were thin sections prepared at NASA Johnson Space Center and cleaned with isopropyl alcohol before being carbon coated for Scanning Electron Microscope (SEM) analysis. The 12038,263 and 12063,330 samples were chips mounted in EPOTEK epoxy resin blocks at Birkbeck College, University of London. Initial Back Scattered Electron (BSE) and elemental mapping of the four thin sections was performed at the Open University with a Quanta 3D Focused Ion Beam (FIB) Scanning Electron Microscope (SEM), while 12038,263 and 12063,330 were mapped at Birkbeck College using a JEOL JXA-8100 electron microprobe (Fig. A.1). Both instruments were fitted with Oxford Instruments INCA energy dispersive X-ray (EDS) detectors. Acquisition of additional BSE and elemental maps was performed with a Quanta 650 Field Emission Gun (FEG) SEM and accompanying Oxford Instruments EDS detector at Stockholm University. For all three SEM setups, the mapping and analysis of the samples was conducted with an electron beam accelerating voltage of 15-20 kV at a working distance of 10-15 mm. The BSE and element maps were then used to identify phases for SIMS analyses; these included plagioclase and pyroxene grains, as well as accessory phases (such as K-Feldspar and K-rich glass; Fig. A.2), which were identified based on regions of high-K and high-Si.

Following SEM documentation of the samples and prior to the SIMS analyses, the samples were cleaned with isopropyl alcohol before applying a 30 nm thick gold coat. The Pb isotopic compositions of various phases (Table B.1) were determined over three analytical sessions using a CAMECA IMS 1280 ion microprobe at the NordSIMS facility in the Swedish Museum of Natural History, Stockholm, using a methodology similar to that outlined in previous studies (Whitehouse et al. 2005; Nemchin et al. 2011; Bellucci et al. 2015). Apertures in the primary column were used to generate a slightly

elliptical O_2^- sample probe with dimensions appropriate to the target. The smaller accessory phases (including K-feldspar and K-rich glass) were analysed using a ~10 µm spot (beam current ca. 2-3 nA), while larger accessory phases and plagioclase grains were analysed with either a ~20 µm spot (beam current ca. 10-12 nA), or a ~30 µm spot (ca. 19-20 nA) (Fig. A.2). Prior to each measurement, an area of 20-35 µm around the spot location was rastered for 60 seconds in order to remove the gold coating and minimise possible surface contamination. The instrument was operated in high-transmission mode, corresponding to a transfer magnification of 160×. In this mode, the field aperture size was chosen to limit the field of view on the sample surface (i.e. the area from which ions will be admitted to the mass spectrometer) to be bigger than the unrastered spot but smaller than the rastered area, further minimising the possibility of surface contamination. The mass spectrometer was operated at a nominal mass resolution of 4860 (M/ΔM), sufficient to resolve Pb from known molecular interferences. An NMR field sensor regulated the stability of the magnetic field. Pb-isotopes were measured simultaneously in multi-collector mode using four low-noise (<0.01 counts per second) ion counting electron multipliers (Hamamatsu 416) with electronically gated deadtimes of 60 ns. Background counts for each channel were measured at regular intervals during each session. The average background counts for each session were used to correct the sample analyses and are presented in Table B.2.

Analyses of the USGS basaltic glass reference material, BCR-2G, were used to correct for mass fractionation and detector gain calibration. The BCR-2G analyses were all within ±5% of the values presented by Woodhead and Hergt (2000), and these deviations were used to generate correction factors for the data. The reproducibility of the BCR-2G analyses for all three sessions were as follows: $^{208}Pb/^{206}Pb$ = 0.63%, 0.46% and 0.38%; $^{207}Pb/^{206}Pb$ = 0.24%, 1.27% and 0.19%; $^{208}Pb/^{204}Pb$ = 0.81%, 1.48% and 0.24%; $^{207}Pb/^{204}Pb$ = 1.18%, 0.86% and 0.33%; $^{206}Pb/^{204}Pb$ = 0.95%, 1.91% and 0.14% (reported as 2σ standard deviations from the average values for each session). Data were then processed using in-house SIMS data reduction spreadsheets and the Excel add-in Isoplot (version 4.15; Ludwig 2008).

Follow-up SIMS analyses provided an approximate measure of the $^{238}U/^{208}Pb$ ratios for multiple spots within several of the samples. These were performed using a 4-5 nA O^{2-} primary beam to produce a slightly elliptical ~10 µm spot on the surface of the sample, within the areas previously analysed for Pb isotopic compositions. The $^{238}U/^{208}Pb$ analyses were made in mono-collector mode, with each analysis preceded by a series of automated centering and optimization procedures using the ^{208}Pb peak. The data collection routine then consisted of 30 cycles through the ^{208}Pb and ^{238}U masses. Note, these measurements were not calibrated with representative standards for the individual minerals measured and are simply used here to provide an indication of the $^{238}U/^{208}Pb$ ratio. They should not, for example, be used to construct U/Pb isochrons.

2.2. Data processing

The SIMS technique was applied to generate a large dataset (Fig. A.3; Table B.1), which has been filtered to discriminate obvious terrestrial contamination, yield isochrons and define initial Pb isotope compositions (Figs. 1; A.3). The Pb isotopic compositions determined for each of the samples are interpreted as representing mixtures between three main components: [1] an initial Pb component incorporated into the rock at the time of crystallization; [2] Pb generated by the *in situ* decay of U; and [3] terrestrial contamination. On a $^{207}Pb/^{206}Pb$ vs. $^{204}Pb/^{206}Pb$ plot, the trend between the first two components is a primary isochron and is defined by the points with the lowest $^{204}Pb/^{206}Pb$ values for particular $^{207}Pb/^{206}Pb$ ratios that form the steepest trend on the diagram. This isochron was used to determine the crystallization age of each sample. The presence of terrestrial contamination will lead to points falling to the right of the isochron and towards the composition of modern terrestrial Pb (Stacey and Kramers 1975). As such, the data for each sample were filtered so as to define a statistically significant isochron (MSWD <2; probability of fit >0.1) on a $^{207}Pb/^{206}Pb$ vs. $^{204}Pb/^{206}Pb$ plot with no analytical points lying to the left of it (Fig. 1). The analyses removed during this filtering process include those with the lowest count rates and, consequently, the largest analytical uncertainties (Fig. A.4; Table B.1). An exception to this was the Apollo 15 KREEP basalt sample (15386,46), for which it was not possible to obtain an isochron with an MSWD <5.3 based on the current dataset. In addition to the three main components discussed, some contribution to the measured Pb isotope compositions

may in theory also come from meteoritic material and contamination from an old (>3.9 Ga) lunar Pb component identified in previous studies (Tera and Wasserburg 1974; Borg et al. 2011), which has been interpreted as being distributed across the lunar surface due to volatilization of Pb by impacts during the period of heavy bombardment that characterised early lunar history. A conceivable mechanism for introducing one or both of these components into unaltered basaltic samples that postdate this period is through interaction of the lower part of the basaltic flow with the lunar surface during the basalt extrusion. However, the bulk of the basaltic flow is unlikely to have been affected. Furthermore, mixing of these components during eruption of the basalts will have resulted in an effective mixing and homogenization of different initial Pb components on the sample scale and will, therefore, have no effect on the way the Pb/Pb isochrons are constrained. The possible presence of such contamination may be confirmed or disproved with further analyses of samples interpreted to represent different parts of individual basalt flows.

The data were also filtered in order to remove any analyses where the count rates for any of the Pb isotopes were very low and effectively below detection limits (<3× the measured background count rates; Tables B.1; B.2). In the dataset presented here, it is also notable that the analyses with the largest analytical errors and lowest Pb counts are also typically those with the highest $^{204}Pb/^{206}Pb$ ratios (Fig. A.3; Table B.1). This is interpreted as evidence that the points with the lowest counts of Pb are also those that are most affected by the presence of terrestrial contamination.

3. Results

The Apollo 11 basalt (10044) yields a crystallization age of 3688±5 Ma, while the three Apollo 12 basalts (12038, 12039 and 12063) have crystallization ages of 3242±13 Ma, 3129±10 Ma and 3193±11 Ma, respectively (Fig. 2). A crystallization age of 3905±8 Ma is determined for the high-Al (and KREEP-rich) Apollo 14 basalt (14072), and 3884±76 Ma for the Apollo 15 KREEP basalt (15386; Fig. 2). The uncertainties for each of these ages are quoted at the 2σ level.

For 10044, the analysis with the highest $^{207}Pb/^{206}Pb$ ratio (and therefore the most likely to represent an initial Pb component) is within error of several analyses obtained in a separate study for a similarly

aged, low-K, ilmenite basalt 10047 (Fig. 2a; Rasmussen et al. 2008). As such, we have taken an average of the analyses in our dataset with the highest $^{207}Pb/^{206}Pb$ ratios and those in the data presented by Rasmussen et al. (2008), as being the best indication of the initial Pb component in the Apollo 11 ilmenite basalt suite. In 12038 and 12063, the highest $^{207}Pb/^{206}Pb$ compositions are represented by a single measurement in each sample. Therefore, we have no option but to use these compositions as the closest estimate for the initial Pb component in each sample. Although these initial Pb values may slightly underestimate the $^{207}Pb/^{206}Pb$ and $^{204}Pb/^{206}Pb$ ratios of the true initial composition, they nonetheless provide the lowest possible limit. In 12039, we interpret a clustering of K-feldspar compositions as representing the initial Pb component of the sample (Fig. 2c). A weighted average of all analyses from this cluster was taken as the best estimate for this initial Pb composition. For 14072, three plagioclase analyses were interpreted as providing the closest approximation to initial Pb compositions (Fig. 2e). In the case of 15386, the analyses with the highest $^{207}Pb/^{206}Pb$ ratios fall significantly to the right of the sample isochron in the $^{207}Pb/^{206}Pb$ vs. $^{204}Pb/^{206}Pb$ coordinate space (Fig. 3). This is interpreted to be a result of minor terrestrial contamination. Consequently, an initial Pb composition for this sample has been estimated by calculating the intercept between the sample isochron and the mixing trend between the initial Pb component and the terrestrial contaminant (Fig. 3).

The measured $^{238}U/^{208}Pb$ ratios determined in several of the samples provide a first order check that the obtained Pb isotopic compositions do indeed represent a mixture between initial and radiogenic Pb. In the locations interpreted as having Pb isotopic compositions closer to initial values, the U content is confirmed as being lower than in the locations interpreted as containing radiogenic Pb supported by the *in situ* decay of U (Fig. 4).

4. Discussion

4.1. Comparison of basalt ages with previous studies

The crystallization ages determined here are in broad agreement with previous studies (Fig. 5; Table B.3; cited in the following discussion with 2σ uncertainties). Two separate studies of 10044

226 determined Rb-Sr ages of 3700±70 Ma and 3710±110 Ma (Albee et al. 1970; Papanastassiou and
227 Wasserburg 1971). Early analyses of this sample also determined a range of ^{39}Ar-^{40}Ar plateau ages;
228 3740±50 Ma, 4000±70 Ma and 3710±40 Ma (Turner 1970; Davis et al. 1971; Guggisberg et al. 1979).
229 Note, these ^{39}Ar-^{40}Ar and Rb-Sr ages reflect the original reported values and have not been
230 recalculated for updated monitor ages and decay constants. More recently, Tartèse *et al.* (2013)
231 determined a ^{207}Pb/^{206}Pb age of 3722±11 Ma for the sample with *in situ* analyses of tranquillityite. The
232 tranquillityite ^{207}Pb/^{206}Pb age is significantly older than the age determined in this study for 10044
233 (3688±5 Ma), but was determined from the weighted average of ^{207}Pb/^{206}Pb ages from very radiogenic
234 Pb isotope compositions, which were not corrected for the presence of initial lunar Pb. These
235 compositions all lie at the extreme lower end of the isochron in Fig. 2a. If the tranquillityite data from
236 Tartèse et al. (2013) are combined with those from this study, both datasets fall on the same isochron
237 and an overall age of 3687±4 Ma (MSWD = 1.3) is obtained (Fig. 6).

238 Previous estimates for the crystallization age of the Apollo 12 feldspathic basalt (12038) were made
239 using Rb-Sr isochrons (3280±210 Ma and 3350±90 Ma; Compston et al. 1971; Nyquist et al. 1981)
240 and Sm-Nd analyses (3280±230 Ma; Nyquist et al. 1981). The crystallization age of the pigeonite
241 basalt, 12039, was also determined by the Rb-Sr method (3190±60 Ma; Nyquist et al. 1979) and Sm-
242 Nd analyses (3200±50 Ma; Nyquist et al. 1979). The ilmenite basalt, 12063, has been dated in two
243 separate Rb-Sr studies, yielding ages of 3340±100 Ma and 3300±130 Ma (Murthy et al. 1971;
244 Papanastassiou and Wasserburg 1971).

245 Early analyses of 14072 determined a Rb-Sr age of 3990±90 Ma (Compston et al. 1972) and a ^{39}Ar-
246 ^{40}Ar age of 4040±50 Ma (York et al. 1972; uncorrected for new monitor ages and decay constants).
247 The crystallization age of the Apollo 15 KREEP basalt sample, 15386, was first determined by Rb-Sr
248 analyses as 3940±10 Ma (Nyquist et al. 1975). A slightly younger, but consistent Sm-Nd age of
249 3850±80 Ma was determined by Carlson and Lugmair (1979). This age of ~3800-3900 Ma is common
250 in Apollo 15 KREEP basalt samples and has, therefore, been interpreted as representing a period of
251 widespread KREEP volcanism in the nearside Procellarum KREEP Terrane (Carlson and Lugmair
252 1979; Taylor et al. 2012).

4.2. Pb isotope source reservoir evolution models

The initial Pb compositions estimated for all the investigated samples are extremely radiogenic, indicating prolonged growth of radiogenic Pb in high-μ reservoirs, which is consistent with the hypothesis that the Moon experienced profound Pb-loss during it's early evolution. Although single stage model ages are clearly an oversimplification of the true Pb isotope evolution of lunar reservoirs, they can provide an estimate of the time when such high-μ reservoirs were established, providing that there was no significant change in the μ-values of the different reservoirs since the initial loss of Pb from the Moon. These model ages were calculated for the source reservoirs of each of the samples based on the obtained Pb/Pb isochron ages and initial Pb isotope compositions, giving: 4525±32 Ma for 10044, 4423±20 Ma for 12038, 4466±10 Ma for 12039, 4417±20 Ma for 12063, 4423±77 Ma for 14072 and 4384±63 Ma for 15386 (all uncertainties are 2σ). The scatter of these model ages indicates that the evolution of Pb recorded by the analysed samples cannot be explained by a simple single differentiation event on the Moon that coincided with its formation and simultaneously resulted in the overall Pb loss from the Moon and differentiation of the lunar mantle into several reservoirs with distinct μ-values.

Fortunately, Pb isotopes also offer an opportunity to evaluate two-stage models, with the advantage of gaining additional information related to the Pb isotope evolution of the Moon, with an assumption that the formation of the Moon and its differentiation are separated by some time exceeding the errors defined by the analytical uncertainties. These two-stage source reservoir Pb evolution models were calculated, assuming the sources of mare basalts and the primordial KREEP reservoir (i.e. urKREEP; Warren and Wasson 1979) differentiated at approximately the same time (t_1) from a single primordial lunar reservoir with a common μ-value (μ_1), which acquired its Pb isotope composition as a result of radioactive decay before differentiation (between t_0 and t_1; Fig. 7a). Starting with the Pb isotope composition of Canyon Diablo Troilite (CDT values; Göpel et al. 1985), a two-stage model was calculated for a range of t_0 times (between 4567 and 4400 Ma) in order to obtain corresponding values for μ_1 (primordial lunar reservoir) and μ_2 (six values for the source of each basalt investigated), as well as the age of differentiation and the Pb isotope composition at this time (see Appendix C for

discussion of model calculations). The model was calculated using nonlinear regression fitting function in Matlab in order to optimize the fit with the ages and initial Pb compositions of all investigated samples. These calculations were initially performed assuming that the μ-values of the Earth-Moon precursor materials were low enough that there was no significant evolution of the Pb isotope compositions away from CDT values between 4567 Ma (Connelly et al. 2012) and t_0. Additional model runs were then performed assuming a range of precursor μ-values, allowing for Pb isotope compositions more radiogenic than CDT prior to the formation of the Moon. The results (Figs. 7b and 8a) indicate that changing t_0 does not produce any significant variation in time of differentiation, with t_1 being centred at 4376±18 Ma (2σ) for t_0 of 4500 Ma and estimates for all other t_0 values ranging within this 18 Ma uncertainty (Table B.4). A similarly limited variability is observed for the Pb isotope composition at the time of differentiation ($^{204}Pb/^{206}Pb$ = 0.036±0.004 and $^{207}Pb/^{206}Pb$ = 1.59±0.02; Fig. 7b) and, as a consequence, the μ_2-values (372±14 for 10044, 534±4 for 12038, 643±4 for 12039, 419±7 for 12063, 2604±185 for 14072 and 3675±271 for 15386; Table B.4). The μ_1-value is the only parameter that changes significantly with changing the model start time (274±50 when t_0 = 4567 Ma and 1063±184 when t_0 = 4425 Ma; Fig. 8a). The uncertainties on these model values are quoted at the 2σ level. The model calculation becomes less stable when t_0 moves closer to t_1, indicating that it is becoming increasingly difficult to fit all the analytical data into a two-stage model. This loss of stability is reflected in the increased uncertainty of μ_1 estimates corresponding to the younger t_0 values (e.g. μ_1 = 1557±727 when t_0 = 4400 Ma; Fig. 8a; Table B.4).

Initial $^{208}Pb/^{204}Pb$ compositions were determined for all of the mare basalts and 14072 (it was not possible to determine the initial $^{208}Pb/^{204}Pb$ composition of 15386 with the current data set). Within the uncertainties of these initial compositions, the samples can all be modelled as having evolved from t_1 (4376 Ma) until their respective crystallization ages with a κ-value ($^{232}Th/^{238}U$) of 3.90±0.64 (Fig. 9), which is similar to estimates for the terrestrial and martian systems (Zartmann and Doe 1981; Kramers and Tolstikhin 1997; Bellucci et al. 2015).

4.3. Model interpretation and implications

Two-stage Pb evolution models, such as the one proposed by Stacey and Kramers (1975), have been an important initial step in the understanding of terrestrial evolution and chemical differentiation. Although these models cannot describe the full complexity of the Earth's history, when combined with information obtained from other isotope systems, they have led to the development of the modern field of mantle chemical geodynamics over the past 40 years. The Stacey and Kramers (1975) model is still widely used in all chronological studies to determine composition of initial Pb when applying corrections to the U-Pb data obtained for the principal geochronometers, such as zircon, monazite, titanite etc. Similarly, the Pb evolution model presented here for the Moon is the first step in a better understanding of the dynamics and differentiation of lunar mantle. It is important, therefore, to determine the significance and limitations of the ages and μ-values defined by this model.

4.3.1. μ-value of the Bulk Silicate Moon and implications for the age of the Moon

The two-stage model calculations based on the currently available data cannot provide a unique and precise set of values for the age of the Moon and the μ-value of the Bulk Silicate Moon (i.e. μ_1) acquired during its formation. Nevertheless, the model highlights the relationship between the time of lunar formation and the μ_1-value (Fig. 8), such that if one of these parameters can be determined independently, the other one would be defined by the Pb isotope systematics described in this study. For example, accepting the recently proposed young age for the Moon (Borg et al. 2011; Carlson et al. 2014; McLeod et al. 2014), requires a comparatively high first stage μ_1-value (1063±184 when t_0 = 4425 Ma or 1557±727 when t_0 = 4400 Ma), as well as a 2-5× decrease of the μ_2-values in the mare basalt sources relative to that of the undifferentiated LMO and a 2-3× increase of the μ_2-values in urKREEP. Conversely, older lunar formation requires more moderate μ_1-values (e.g. 462±46 when t_0 = 4500 Ma), a negligible change in μ-values between the undifferentiated LMO and mare basalt sources, and a 5-10× increase to reach the urKREEP μ_2-values. Regardless of the precise age of the Moon, the model places constraints on LMO crystallization and the formation of major lunar silicate reservoirs (Fig. 8a; Table B.4), as the Pb isotope modelling restricts the range of μ_2-values for both the mare basalt sources (~300 to 700) and urKREEP (~2500 to 3500).

So long as U and Pb partitioning behaviour between melt and the main rock forming minerals is well constrained, any LMO differentiation model that defines a specific set of μ_1-μ_2 relationships will uniquely determine the age of the Moon. While estimates of U and Pb partition coefficients are available (e.g. Green 1994; Bindeman et al. 1998; Bindeman and Davis 2000; Fonseca et al. 2014), to date, no study has determined coefficients for both elements from a single set of experiments. Thus, prediction of the relative behaviour of these elements in magmatic fractionation processes will be imprecise and prevent full application of the Pb-isotope model presented here.

While the two-stage Pb evolution model appears to have the capacity to describe the early evolution of the Moon within the framework of the LMO crystallization sequence, it is necessary to consider several complications, which may violate the model. The estimated first stage μ-value is likely to be an integrated result of several discrete or continuous changes in the U-Pb ratio of the primordial lunar reservoir, rather than a single increase at the starting time of the model. However, achieving a high-μ early in the differentiation history is necessary to attain the observed radiogenic Pb compositions. This supports the conclusion of earlier work that Pb volatility is the major factor in its depletion in the Moon. Sequestration of Pb into the lunar core as it formed could provide one alternative way to increase the μ-value of the primordial lunar reservoir. In the case of the Earth, formation of a volumetrically large core only generated, at most, a ~10× increase in terrestrial mantle μ-values (Kramers and Tolstikhin 1997). Additionally, the segregation of the Martian core did not increase the μ-value of the Martian mantle by a substantial amount (Bellucci et al. 2015). By comparison, the Moon has a relatively small core (~20% of its mean radius; Weber et al. 2011), making it impossible by mass balance to explain the high-μ (exceeding 300-400) by core segregation, which instead would have more likely resulted in a comparatively minor, and currently unresolved, μ-value increase during the first stage of the model (between μ_1-μ_2).

An alternative to profound Pb loss during the formation of the Moon, which can possibly explain the Pb isotope compositions observed in lunar samples, is to consider high-μ precursor material, for example, a high-μ impactor colliding with the Earth in the Moon forming giant impact. This scenario would allow for more radiogenic Pb isotope compositions to have evolved prior to t_0. In a simplistic

359 case where the precursor material is considered as a single reservoir (i.e. neglecting the effects of
360 mixing between the early Earth and the giant impactor), the Pb isotope compositions can be explained
361 with a μ_1-value of 791±301 when t_0 is 4400 Ma, if the precursor has a μ-value of 200 and formed at
362 about the same time as the Solar System (Fig. 8a). However, giant impact models commonly predict
363 that the primordial Moon would contain tens of percent (by mass) of material from the Earth (Canup
364 and Asphaug 2001). Since a high-μ impactor would be expected to have a low concentration of Pb due
365 to the volatile nature of Pb and refractory nature of U, even small amounts (e.g. 10%) of terrestrial
366 material (assuming a μ-value of ~8) will dominate the Pb budget of any mix with such an impactor.
367 For example, even an impactor μ-value of 2000 (which seems highly unlikely given the comparatively
368 low μ-values observed in other planetary bodies; Zartman and Doe 1981; Kramers and Tolstikhin
369 1997; Gaffney et al. 2007b; Amelin 2008; Bellucci et al. 2015), would be little different to CDT
370 starting composition (Fig. 8b), unless a high-μ early Earth is considered (Albarède 2009).

371 #### 4.3.2. Reservoir differentiation and Crystallization of the Lunar Magma Ocean

372 The two isotopically distinct groups of reservoirs predicted in the second stage of this model have
373 about a five-fold difference in μ-value. One is the source of the mare basalts and the other is a
374 KREEP-rich reservoir (urKREEP: Warren and Wasson 1979). Both are anticipated to form in a classic
375 LMO model crystallization sequence (e.g. Wood et al. 1970; Elkins-Tanton et al. 2011). While the
376 urKREEP represents a very small (a few percent maximum) portion of the LMO residual melt, the
377 source of the mare basalts is considered to be an olivine-pyroxene cumulate formed during LMO
378 crystallization (e.g. Wood et al. 1970; Snyder et al. 1992). Having estimates of the μ-values for these
379 reservoirs allows for some simple first order constraints to be made in relation to the differentiation of
380 the LMO based on the known behaviour of U and Pb in magmatic systems, even though exact
381 partition coefficients for these elements are not very well constrained. Both are considered to be very
382 incompatible with the available estimates of partition coefficients between most rock forming minerals
383 and basaltic melt falling below 0.01 (e.g. Green 1994; Fonseca et al. 2014). If that is the case, more
384 than 90% of the original U and Pb will have remained in the residual melt, even after 99.99% of the
385 LMO crystallized. Therefore, in the absence of phases concentrating significant amounts of Pb,

386 fractional crystallization of the LMO appears not to be capable of changing the residual melt μ-value
387 by more than about 10%, and certainly not the 2-10× increase predicted by the model for urKREEP,
388 unless the initial μ-value that the Moon acquired during its formation was similar to that estimated for
389 urKREEP. Alternatively, the observed increase in the urKREEP μ-value could be unrelated to the
390 magmatic differentiation process and explained instead by a significant loss of Pb from the residual
391 LMO liquid. For example, degassing of the residual LMO liquid has been proposed following
392 comparative studies of Cl isotope signatures in mare basalts and KREEP-rich rocks (Boyce et al. 2015;
393 Barnes et al. 2016).

394 Two groups of minerals provide likely candidates as Pb sinks in the assemblages crystallizing from the
395 LMO; sulfides and feldspars. If all U stays in the residual melt, fractionation of an assemblage with a
396 bulk Pb partition coefficient of around 0.25 is required to achieve a 2× increase in the μ-value of the
397 remaining 5% of melt. Taking into account that it is likely only part of the entire LMO cumulate pile is
398 characterized by increased Pb concentrations, a partition coefficient of 0.4-0.5 would be more realistic
399 to explain the urKREEP μ-value. Fractionation of sulfides during LMO crystallization is feasible, but
400 the lack of samples representing this process in the existing collection of lunar rocks means that this
401 possibility cannot be tested in great detail. However, the FAN samples thought to represent the
402 primary feldspathic crust are an important product of LMO crystallization. Results of Pb isotope
403 studies of the FAN samples (e.g. Premo et al. 1999) indicate that plagioclase in these samples has a
404 range of μ-values between ~1 and 30, supporting the assumption that this mineral can extract two
405 orders of magnitude more Pb than U out of its parent melt. This is further supported by studies of U
406 and Pb partitioning in plagioclase (Bindeman et al. 1998; Bindeman and Davis 2000).

407 A number of recent chronological results are easier to explain if the observed increase in the μ-value
408 characterising KREEP-rich materials is linked to FAN formation, in particular younger ages of some
409 FAN samples similar to the Nd and Hf model ages of KREEP-rich samples (Borg et al. 2011; Carlson
410 et al. 2014; McLeod et al. 2014). In fact, of all the related analytical data recently obtained, the most
411 difficult to explain is the range of ^{142}Nd model ages of several FAN samples presented by Boyet et al.
412 (2015), which indirectly supports protracted crystallization of the anorthositic lunar crust, and the

large ^{142}Nd deficit in one sample (62255), which is impossible to explain if it formed after ~4440 Ma. The two-stage Pb model likely provides a good approximation for the time (4376±18 Ma) for the crystallization of the mineral assemblage that ultimately resulted in FAN formation as well as producing the enrichment of incompatible elements in the residual melt, leading to the high-μ isotopic signature of urKREEP. This Pb model age is further supported by a majority of the Nd and Hf model ages for similar rocks (Borg et al. 2011; Carlson et al. 2014; McLeod et al. 2014), and may not date the precise timing of urKREEP (and FAN) formation, but rather an average time of a potentially complex process that could have extended over a few million to a few tens of millions of years.

As discussed in the previous section (4.3.1), since U and Pb partitioning behaviour is not well understood, the two-stage Pb model presented here is currently not in conflict with either an "old" or a "young" Moon. Resolution of the conflict regarding the formation of the Moon has implications for defining a unique time for the formation of the mare basalt sources. If the Moon is "old", and the μ-values of the mare basalt sources are similar to that of the primordial lunar reservoir, then the time of mare basalt source formation is difficult to determine as it will effectively be invisible within the two-stage model, where formation of urKREEP and FAN dominates the fractionation of U and Pb in the LMO. More incompatible behaviour of U (relative to Pb), will imply late formation of both the LMO and the Moon, in which case the 4376±18 Ma age will also encompass the time of mare basalt source formation, satisfying the main assumption of the two-stage model, that the differentiation took place at a single point in time from a previously undifferentiated reservoir.

Similar uncertainty with low-Ti basalts exists in the Nd isotopic dataset. The olivine and pigeonite basalts investigated by McLeod et al. (2014) are not fractionated far enough from the primitive reservoir to provide any definitive differentiation time constraints on their own in the ^{142}Nd-^{143}Nd system. This behaviour is remarkably similar to that of the Pb isotope systematics described above, which indicates that the mare basalt sources do not show a significant change in either their μ-value or Sm-Nd ratio, relative to that of the undifferentiated Moon and, consequently, the model age of differentiation defined by both systems at about 4370-4380 Ma defines the average time of urKREEP differentiation and FAN formation, but not necessarily the separation of the mare basalt sources. As

such, neither the Pb nor Nd isotope systems can be used to determine exactly when these mare basalt mantle sources formed. Strictly speaking the "young" (~4340-4390 Ma) ages in the McLeod et al. (2014) data are defined by an Apollo 15 KREEP basalt and Apollo 17 high-Ti basalts, which are assumed to represent some of the final differentiates of the LMO, i.e. ilmenite-rich cumulates and urKREEP (e.g. Warren and Wasson 1979; Snyder et al. 1992).

5. Conclusions

By using SIMS analyses to determine the Pb isotope compositions of multiple phases in lunar basalts, crystallization ages have been determined that are both consistent with previous studies and, in most cases, significantly more precise. In addition to these ages, the data have been used to constrain the isotopic compositions of Pb incorporated into the basalts when they crystallized, from which a two-stage model has been constructed for the Pb-isotopic evolution of major lunar silicate reservoirs. This model is necessarily a simplification of the early magmatic differentiation of the Moon, omitting the effects of processes such as core segregation. Nonetheless, it provides a framework upon which subsequent studies can build, and several important constraints for the timing of key stages in this evolution and Pb isotope compositions at these stages. In principle, the model is capable of resolving uncertainty over the age of the Moon, but this requires better knowledge of U and Pb partitioning behaviour in magmatic systems. The Pb isotope data support a major magmatic event on the Moon at 4376±18 Ma, possibly representing the average age of urKREEP and FAN formation. Following this event the mare basalt sources evolved with relatively low μ-values (370-640), while the KREEP reservoir acquired a significantly larger μ-value (2600-3675).

Acknowledgments: The authors thank NASA and CAPTEM for allocation of samples, and the Apollo astronauts who risked their lives to collect them. This work was funded by grants from the Knut and Alice Wallenberg Foundation and the Swedish Research Council to M.J.W. and A.A.N. This work was also partially supported by the UK Science and Technology Facilities Council (STFC) grants to M.A. (ST/I001298/1 and ST/L000776/1) and KHJ (ST/M001253/1). The NordSIMS facility is

operated under a joint Nordic agreement; this is NordSIMS publication ***. The research has made use of NASA's Astrophysics Data System.

References:

Albee, A. L., Burnett, D. S., Chodos, A. A., Eugster, O. J., Huneke, J. C., Papanastassiou, D. A., Podosek, F. A., Russ, G. P., Sanz, H. G., Tera, F. & Wasserburg, G. J. Ages, Irradiation History, and Chemical Composition of Lunar Rocks from the Sea of Tranquillity. *Science* **167,** 463-466 (1970).

Albarède F. Volatile accretion history of the terrestrial planets and dynamic implications. *Nature* **461,** 1227-1233 (2009),

Amelin, Y. The U-Pb systematics of angrite Sahara 99555. *Geochim. Cosmochim. Acta* **72,** 4874-4885 (2008).

Avice, G. & Marty, B. The iodine–plutonium–xenon age of the Moon–Earth system revisited. *Phil-Trans. R. Soc. A.* **372,** 20130260 (2014).

Barnes, J. J., Tartèse, R., Anand, M., McCubbin, F. M., Neal, C. R. & Franchi, I. A. Early degassing of lunar urKREEP by crust-breaching impact(s). *Earth Planet. Sci. Lett.* **447,** 84-94 (2016).

Bellucci, J. J., Nemchin, A. A., Whitehouse, M. J., Snape, J. F., Bland, P. A. & Benedix G. K. The Pb isotopic evolution of the Martian mantle constrained by initial Pb in Martian meteorites. *J. Geophys. Res. (Planets)* **120,** 2224-2240 (2015).

Bindeman, I. N. & Davis, A. M. Trace element partitioning between plagioclase and melt: investigation of dopant influence on partition behaviour. *Geochim. Cosmochim. Acta* **64,** 2863-2878 (2000).

Bindeman, I. N., Davis, A. M. & Drake, M. J. Ion Microprobe Study of Plagioclase-Basalt Partition Experiments at Natural Concentration Levels of Trace Elements. *Geochim. Cosmochim. Acta* **62,** 1175-1193 (1998).

Borg, L. E., Connelly, J. N., Boyet, M. & Carlson, R. W. Chronological evidence that the Moon is either young or did not have a global magma ocean. *Nature* **477,** 70-72 (2011).

491 Borg, L. E., Gaffney, A. M. & Shearer, C. K. A review of lunar chronology revealing a preponderance
492 of 4.34–4.37 Ga ages. *Meteorit. Planet. Sci.* **50,** 715-732 (2015).

493 Boyce, J. W., Treiman, A. H., Guan, Y., Eiler, J. M., Gross, J., Greenwood, J. P. & Stolper, E. M. The
494 chlorine isotope fingerprint of the lunar magma ocean. *Science Advances* **1,** e1500380-e1500380.

495 Boyet, M., Carlson, R. W., Borg, L. E. & Horan, M. Sm–Nd systematics of lunar ferroan anorthositic
496 suite rocks: Constraints on lunar crust formation. *Geochim. Cosmochim. Acta* **148,** 203-218 (2015).

497 Canup, R. M. & Asphaug, E. Origin of the Moon in a giant impact near the end of the Earth's
498 formation. *Nature* **412,** 708-712 (2001).

499 Carlson, R. W. & Lugmair, G. W. Sm-Nd constraints on early lunar differentiation and the evolution
500 of KREEP. *Earth Planet. Sci. Lett.* **45,** 123-132 (1979).

501 Carlson, R. W., Borg, L. E., Gaffney, A. M. & Boyet, M. Rb-Sr, Sm-Nd and Lu-Hf isotope
502 systematics of the lunar Mg-suite: the age of the lunar crust and its relation to the time of Moon
503 formation. *Phil- Trans. R. Soc. A.* **372,** 20130246 (2014).

504 Compston, W., Berry, H., Vernon, M. J., Chappell, B. W. & Kaye, M. J. Rubidium-strontium
505 chronology and chemistry of lunar material from the Ocean of Storms. *Proc. 2nd Lunar Sci. Conf.* **2,**
506 1471-1485 (1971).

507 Compston, W., Vernon, M. J., Berry, H., Rudowski, R., Gray, C. M. & Ware, N. Apollo 14 mineral
508 ages and the thermal history of the Fra Mauro formation. *Proc. 3rd Lunar Planet. Sci. Conf.* **2,** 1487-
509 1501 (1972).

510 Connelly, J. N., Bizzarro, M., Krot, A. N., Nordlund, Å., Wielandt, D. & Ivanov, M. A. The Absolute
511 Chronology and Thermal Processing of Solids in the Solar Protoplanetary Disk. *Science* **338,** 651-655
512 (2012).

513 Davis, P. K., Lewis, R. S. & Reynolds, J. H. Stepwise heating analyses of rare gases from pile-
514 irradiated rocks 10044 and 10057. *Proc. 2nd Lunar Sci. Conf.* **2,** 1693-1703 (1971).

515 Elkins-Tanton, L. T., Burgess, S. & Yin, Q. –Z. The lunar magma ocean: Reconciling the
516 solidification process with lunar petrology and geochronology. *Earth Planet. Sci. Lett.* **304,** 326-336
517 (2011).

518 Floss, C., James, O. B., McGee, J. J. & Crozaz, G. Lunar ferroan anorthosite petrogenesis: Clues from
519 trace element distributions in FAN subgroups. *Geochim. Cosmochim. Acta* **62,** 1255-1283 (1998).

520 Fonseca, R. O. C., Mallmann, G., Sprung, P., Sommer, J. E., Heuser, A., Speelmanns, I. M. &
521 Blanchard, H. Redox controls on tungsten and uranium crystal/silicate melt partitioning and
522 implications for the U/W and Th/W ratio of the lunar mantle. *Earth Planet. Sci. Lett.* **404,** 1-13 (2014).

523 Gaffney, A. M., Borg, L. E. & Asmeron, Y. The origin of geochemical diversity of lunar mantle
524 sources inferred from the combined U-Pb, Rb-Sr, and Sm-Nd isotope systematics of mare basalt
525 10017. *Geochim. Cosmochim. Acta* **71,** 3656-3671 (2007a).

526 Gaffney, A. M., Borg, L. E. & Connelly, J. N. Uranium lead isotope systematics of Mars inferred from
527 the basaltic shergottite QUE 94201. *Geochim. Cosmochim. Acta* **71,** 5016-5031 (2007b).

528 Gaffney, A. M. & Borg, L. E. A young solidification age for the lunar magma ocean. *Geochim.*
529 *Cosmochim. Acta* **140,** 227-240 (2014).

530 Göpel, C., Manhès, G. & Allègre, C. J. U-Pb systematics in iron meteorites - Uniformity of primordial
531 lead. *Geochim. Cosmochim. Acta* **49,** 1681-1695 (1985).Green, T. H. Experimental studies of trace-
532 element partitioning applicable to igneous petrogenesis – Sedona 16 years later. *Chem. Geol.* **117,** 1-
533 36 (1994).

534

535 Guggisberg, S., Eberhardt, P., Geiss, J., Grögler, N., Stettler, A., Brown, G. M. & Peckett, A.
536 Classification of the Apollo-11 mare basalts according to ^{39}Ar-^{40}Ar ages and petrological properties.
537 *Proc. 10th Lunar Sci. Conf.* **1,** 1-39 (1979).

Hartmann, W. K. & Davis, D. R. Satellite-Sized Planetesimals and Lunar Origin. *Icarus* **24,** 504-515 (1975).

Kramers, J. D. & Tolstikhin, I. N. Two terrestrial lead isotope paradoxes, forward transport modelling, core formation and the history of the continental crust. *Chem. Geology* **139,** 75-110 (1997).

Ludwig, K. R. User's Manual for Isoplot 3.60, A geochronological toolkit for Microsoft Excel. Berkeley Geochronological Center Special Publication 4, Berkeley, California: Berkeley Geochronological Center (2008).Stacey, J. S. & Kramers, J. D. Approximation of terrestrial lead isotope evolution by a two-stage model. Earth Planet. Sci. Lett. 26, 207-221 (1975).

McLeod, C. L., Brandon, A. D. & Armytage, R. M. G. Constraints on the formation age and evolution of the Moon from ^{142}Nd-^{143}Nd systematics of Apollo 12 basalts. *Earth Planet. Sci. Lett.* **396,** 179-189 (2014).

Murthy, V. R., Evensen, N. M., Jahn, B. & Coscio, M. R. Jr. Rb-Sr ages and elemental abundances of K, Rb, Sr, and Ba in samples from the Ocean of Storms. *Geochim. Cosmochim. Acta* **35,** 1139-1153 (1971).

Nemchin, A. A., Timms, N., Pidgeon, R., Geisler, T., Reddy, S. & Meyer, C. Timing of crystallization of the lunar magma ocean constrained by the oldest zircon. *Nat. Geosci.* **2,** 133-136 (2009).

Nemchin, A. A., Whitehouse, M. J., Grange, M. L. & Muhling, J. R. On the elusive isotopic composition of lunar Pb. *Geochim. Cosmochim. Acta* **75,** 2940-2964 (2011).

Nyquist, L. E., Bansal, B. M. & Wiesmann, H. Rb-Sr ages and initial ^{87}Sr/^{86}Sr for Apollo 17 basalts and KREEP basalt 15386. *Proc. 6th Lunar Sci. Conf.* **2,** 1445-1465 (1975).

Nyquist, L. E., Shih, C. –Y., Bansal, B. M., Wooden, J. L. & Wiesmann, H. The Sr and Nd isotopic record of Apollo 12 basalts - Implications for lunar geochemical evolution. *Proc. 10th Lunar Sci. Conf.* **1,** 77-114 (1979).

Nyquist, L. E., Wooden, J. L., Shih, C. –Y., Wiesmann, H. & Bansal, B. M. Isotopic and REE studies of lunar basalt 12038 - Implications for petrogenesis of aluminous mare basalts. *Earth Planet. Sci. Lett.* **55,** 335-355 (1981).

564 Papanastassiou, D. A. & Wasserburg, G. J. Lunar chronology and evolution from Rb-Sr studies of
565 Apollo 11 and 12 samples. *Earth Planet. Sci. Lett.* **11,** 37-62 (1971).

566 Pernet-Fisher, J. R. & Joy, K. H. The lunar highlands: old crust, new ideas. *Astronomy & Geophysics*
567 **57,** 1.26-1.30 (2016).

568 Premo, W. R., Tatsumoto, M., Misawa, K., Nakamura, N. and Kita, N. I. (1999) Pb-Isotopic
569 Systematics of Lunar Highland Rocks (>3.9 Ga): Constraints on Early Lunar Evolution. *Int. Geol.*
570 *Rev*. **41**, 95-128.

571 Rasmussen, B., Fletcher, I. R. & Muhling, J. R. Pb-Pb geochronology, petrography and chemistry of
572 Zr-rich accessory minerals (zirconolite, tranquillityite and baddeleyite) in mare basalt 10047.
573 *Geochim. Cosmochim. Acta* **72,** 5799-5818 (2008).

574 Snyder, G. A., Taylor, L. A. & Neal, C. R. A chemical model for generating the sources of mare
575 basalts: Combined equilibrium and fractional crystallization of the lunar magmasphere. *Geochim.*
576 *Cosmochim. Acta* **56,** 3809-3823 (1992).

577 Solomon, S. C. & Longhi, J. Magma oceanography: 1. Thermal evolution. *Proc. 8th Lunar Sci. Conf.*
578 **1,** 583-599 (1977).

579 Stacey, J. S. & Kramers, J. D. Approximation of terrestrial lead isotope evolution by a two-stage
580 model. *Earth Planet. Sci. Lett.* **26,** 207-221 (1975).

581 Tartèse, R., Anand, M. & Delhaye, T. NanoSIMS Pb/Pb dating of tranquillityite in high-Ti lunar
582 basalts: Implications for the chronology of high-Ti volcanism on the Moon. *American Mineralogist*
583 **98,** 1477-1486 (2013).

584 Tatsumoto, M. Age of the moon: An isotopic study of U-Th-Pb systematics of Apollo 11 lunar
585 samples-II. *Geochim. Cosmochim. Acta Supp.* **1,** 1595-1612 (1970).

586 Tatsumoto, M., Premo, W. R. & Unruh, D. M. Origin of lead from green glass of Apollo 15426 - A
587 search for primitive lunar lead. *J. Geophys. Res.* **92,** E361-E371 (1987).

588 Taylor, G. J., Martel, L. M. V. & Spudis, P. D. The Hadley-Apennine KREEP basalt igneous
589 province. *Meteoritics and Planetary Science* **47,** 861-879 (2012).

590 Tera, F. & Wasserburg, G. J. U-Th-Pb systematics in three Apollo 14 basalts and the problem of initial
591 Pb in lunar rocks. *Earth Planet. Sci. Lett.* **14,** 281-304 (1972). Tera, F. & Wasserburg, G. J. U-Th-Pb
592 systematics on lunar rocks and inferences about lunar evolution and the age of the Moon. *Proc. 5th*
593 *Lunar Sci. Conf.* **2,** 1571-1599 (1974).

594

595 Turner, G. ^{40}Ar-^{39}Ar dating of lunar rock samples. *Geochim. Cosmochim. Acta Supp.* **1,** 1665-1684
596 (1970).

597 Warren, P. H. & Wasson, J. T. The origin of KREEP. *Rev. Geophys. Space Phys.* **17,** 73-88 (1979).

598 Weber, R. C., Lin, P. Y., Garnero, E. J., Williams, Q. & Lognonné, P. Seismic Detection of the Lunar
599 Core. *Science* **331,** 309-312 (2011).

600 Whitehouse, M. J., Kamber, B. S., Fedo, C. M. & Lepland, A. Integrated Pb- and S-isotope
601 investigation of sulphide minerals from the early Archaean of southwest Greenland. *Chemical*
602 *Geology* **222,** 112-131 (2005).

603 Wood, J. A., Dickey, J. S., Jr., Marvin, U. B. & Powell, B. N. Lunar anorthosites. *Science* **167,** 602-
604 604 (1970).

605 Woodhead, J. D. & Hergt, J. M. Pb-Isotope Analyses of USGS Reference Materials. Geostand.
606 Geoanal. Res. 24, 33-38 (2000).

607 York, D., Kenyon, W. J. & Doyle, R. J. ^{40}Ar-^{39}Ar ages of Apollo 14 and 15 samples. *Proc. 3rd Lunar*
608 *Sci. Conf.* **2,** 1613-1622 (1972).

609 Zartman, R. E. & Doe, B. R. Plumbotectonics – the model. *Tectonophysics* **75,** 135-162 (1981).

Figure captions

Figure 1. – Schematic illustration of the mixing relationships observed in the datasets between initial Pb, radiogenic Pb and terrestrial contamination, and how these relate to the data filtering procedure.

Figure 2. – $^{207}Pb/^{206}Pb$ vs. $^{204}Pb/^{206}Pb$ plots of filtered datasets from: (a) 10044,645; (b) 12038,263; (c) 12039,44; (d) 12063,330; (e) 14072,61; and (f) 15386,46. The isochrons determined for each sample have been indicated with dashed lines. Also shown are the growth lines for our two-stage model of lunar Pb isotope growth for each sample, from the model Pb isotopic composition at t_1 (4376±18 Ma) to the time of crystallization. Error bars are at 2σ uncertainties.

Figure 3. – $^{207}Pb/^{206}Pb$ vs. $^{204}Pb/^{206}Pb$ plot of complete dataset from 15386,46. In addition to the sample isochron, a second trend (indicating the mixing between the initial Pb component and terrestrial contamination) has been illustrated to demonstrate the calculation of the initial Pb composition for that sample. The modern terrestrial Pb composition illustrated here is taken from the model of Stacey and Kramers (1975).

Figure 4. – Plot of $^{238}U/^{208}Pb$ vs. $^{207}Pb/^{206}Pb$ for points within four of the analysed samples. Note that the $^{238}U/^{208}Pb$ ratio decreases notably for points with a high $^{207}Pb/^{206}Pb$. This indicates that the Pb present in these locations cannot be supported by the *in situ* decay of U and most likely represents the best estimate for the initial Pb composition in each sample. Note, these measurements were not calibrated with representative matrix-matched standards for the individual minerals and are simply used here to provide an indication of the $^{238}U/^{208}Pb$ ratio.

Figure 5. – Comparison of crystallization ages determined in this work (colour symbols) with those of previous studies (black symbols). See main text and Table B.3 for references. Error bars indicate 2σ uncertainties.

Figure 6. – $^{207}Pb/^{206}Pb$ vs. $^{204}Pb/^{206}Pb$ plot comparing the 10044 data from this study with the tranqullityite analyses reported by Tartèse et al. (2013). Error bars indicate 2σ uncertainties.

Figure 7. – (a) The stages of Pb isotopic evolution, starting from Solar System formation, defined by Calcium Aluminium Inclusion formation at 4567 Ma (Connelly et al. 2012), and assuming Canyon Diablo Troilite Pb isotope compositions (CDT; Göpel et al. 1985). The solid arrows indicate stages represented by the two-stage model in this study. (b) $^{207}Pb/^{206}Pb$ vs. $^{204}Pb/^{206}Pb$ plot illustrating the two-stage Pb isotopic growth model with t_0 set at 4500 Ma. Dashed curves indicate the growth curves constructed with the mean model values, while the surrounding fields indicate 2σ uncertainties of these values. The initial Pb compositions determined for each sample are plotted as diamonds, colour coded to the model growth curves. Error bars indicate 2σ uncertainties.

Figure 8. – Model μ-value comparisons. (a) Variation in μ_1- and μ_2-values depending on the two-stage model starting time (t_0). The μ_1-values decrease if Pb isotope evolution in a high-μ (e.g. μ = 200) reservoir prior to t_0 is considered, as is illustrated by the dashed black lines, representing the lower limits of the μ_1-values for a precursor with μ = 0 and μ = 200. (b) The compositions resulting from mixing high-μ materials with low-μ terrestrial material (four filled circles, colour coded to Pb growth curves) lie on an isochron connecting the growth curves at the time of mixing (the 4376 Ma isochron provides an arbitrary example). The growth curves are calculated from Canyon Diablo Troilite Pb isotope composition (CDT; Göpel et al. 1985).

Figure 9. – Plot of the best estimates for the initial $^{208}Pb/^{204}Pb$ compositions plotted against $X = \frac{e^{\lambda_{232}t_1} - e^{\lambda_{232}t_i}}{e^{\lambda_{238}t_1} - e^{\lambda_{238}t_i}} \times \left(\frac{6}{4_i} - \frac{6}{4_1}\right)$, such that the slope of the trend is equal to the κ-value of the system, given that: $\frac{208_{Pb}}{204_{Pb_i}} = \kappa \frac{e^{\lambda_{232}t_1} - e^{\lambda_{232}t_i}}{e^{\lambda_{238}t_1} - e^{\lambda_{238}t_i}} \times \left(\frac{6}{4_i} - \frac{6}{4_1}\right) + \frac{208_{Pb}}{204_{Pb_1}}$

Appendices

Appendix A – Supplementary figures.

Appendix B – Supplementary tables.

Appendix C – Supplementary text.

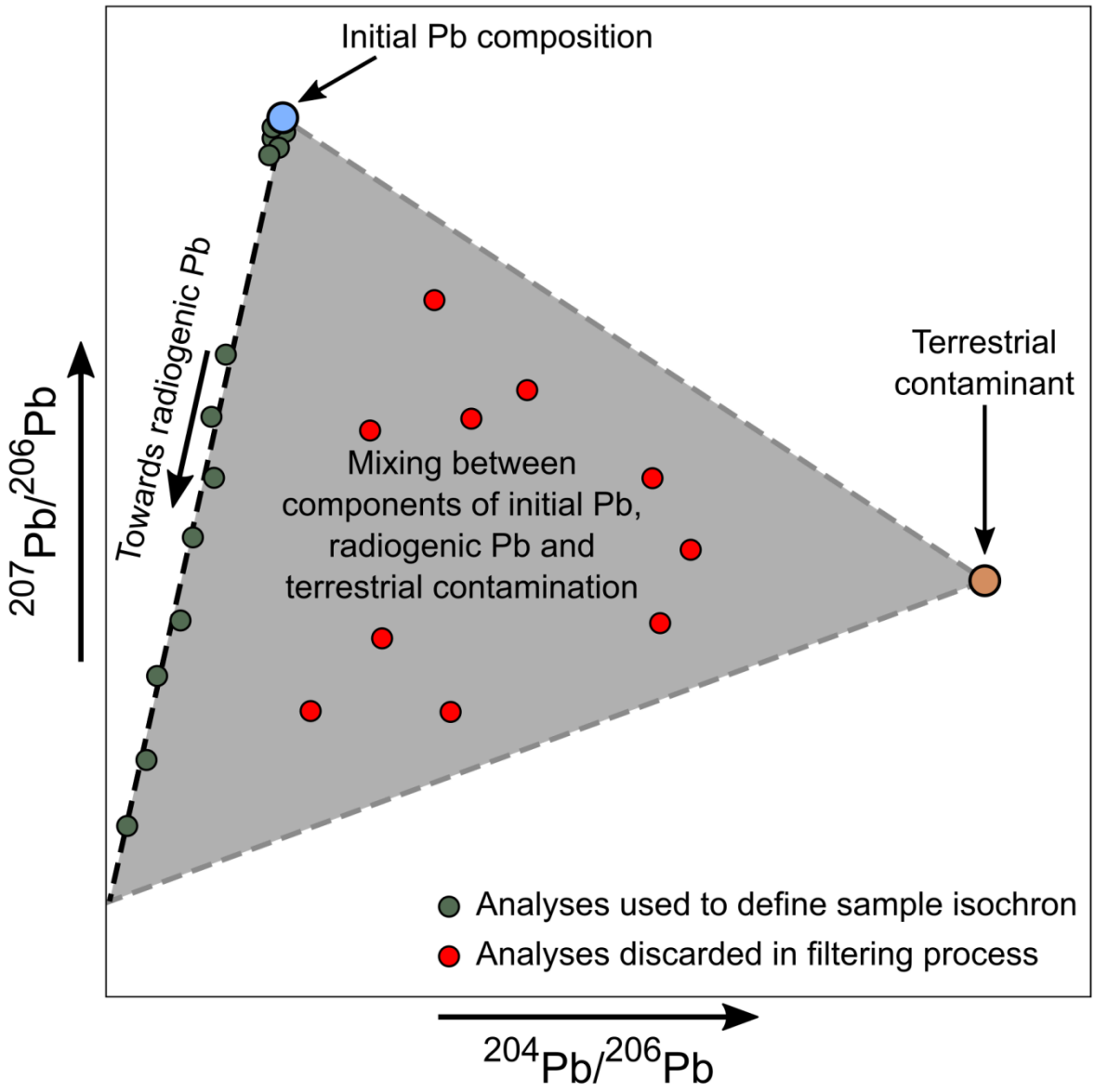

658

659 Figure 1

660

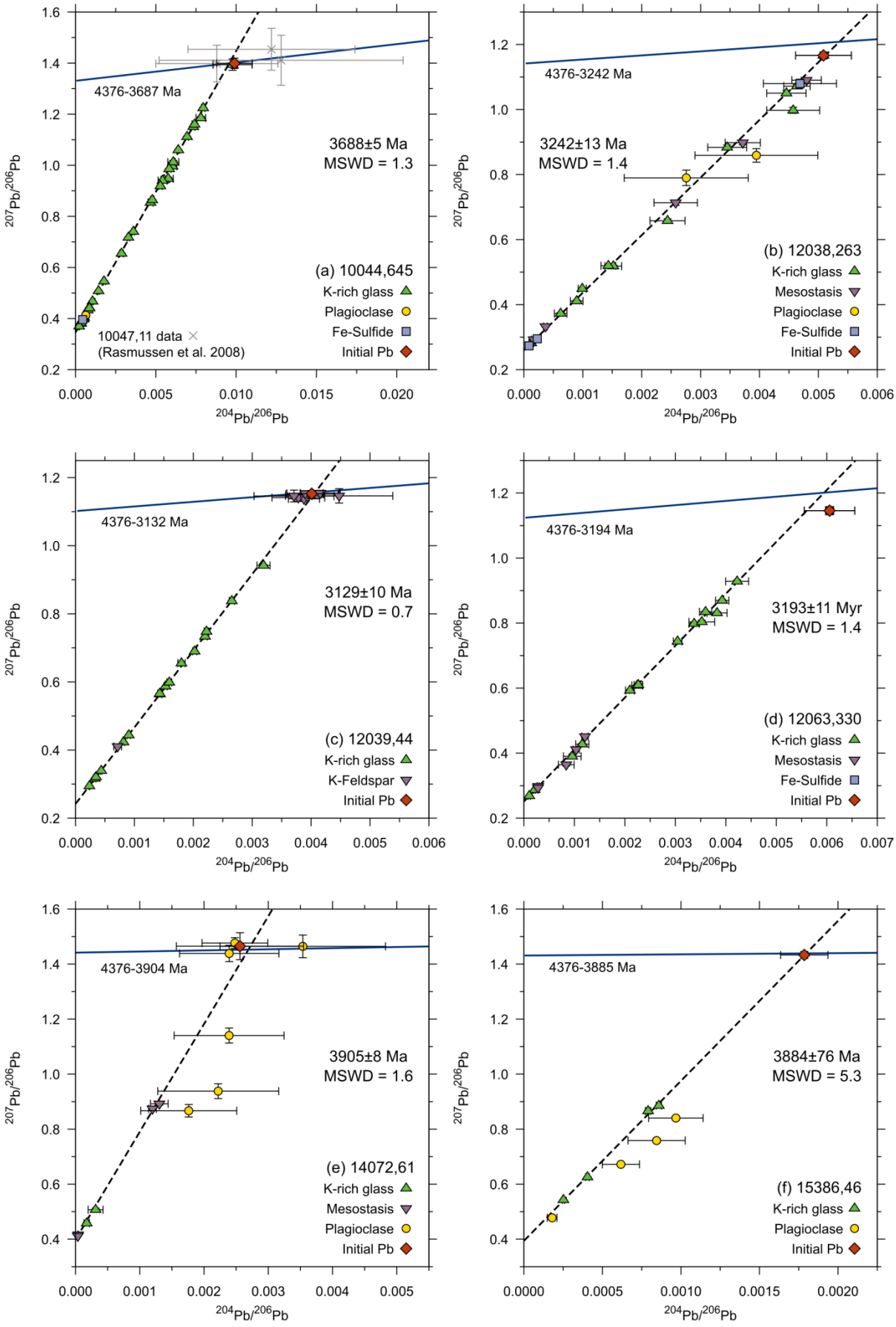

661
662 Figure 2

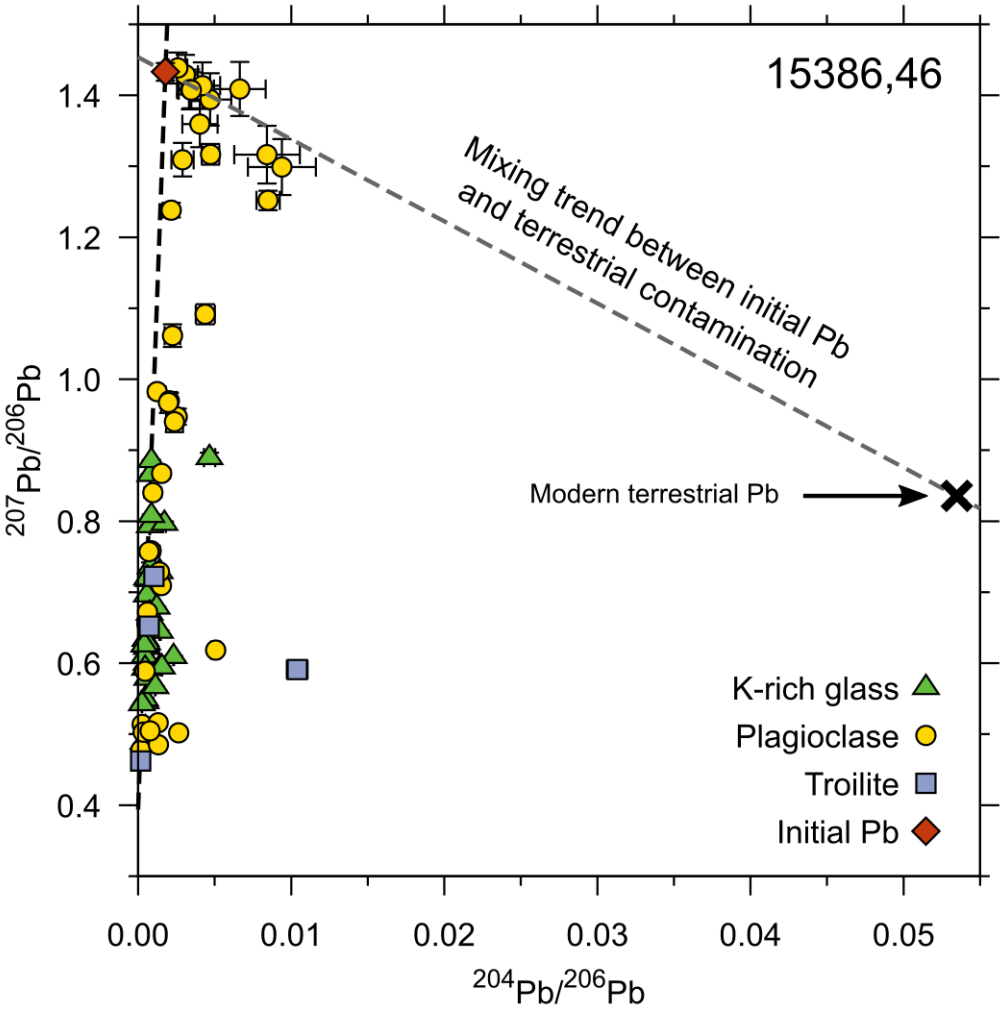

663

664 Figure 3

665

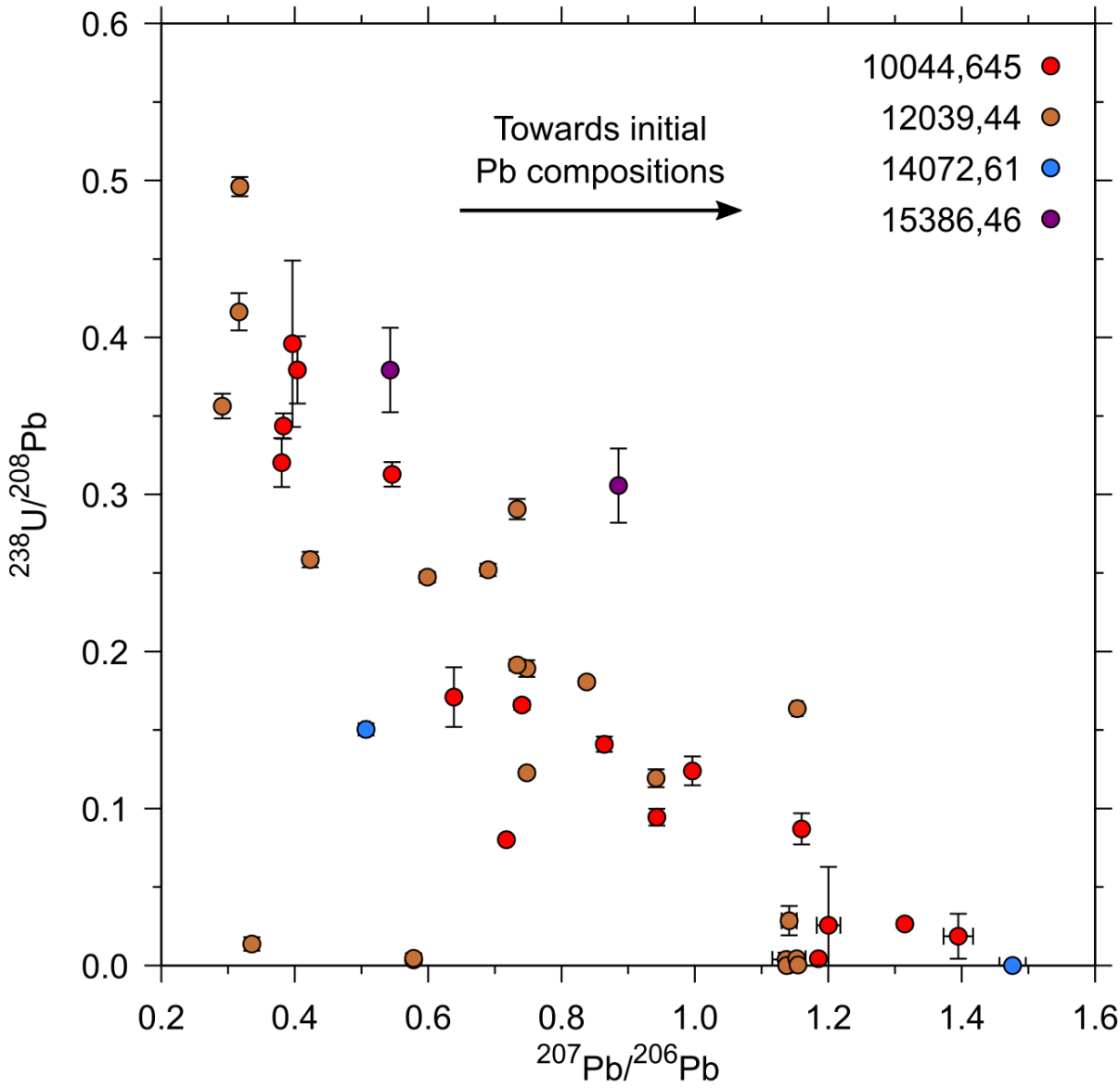

666

667 Figure 4

668

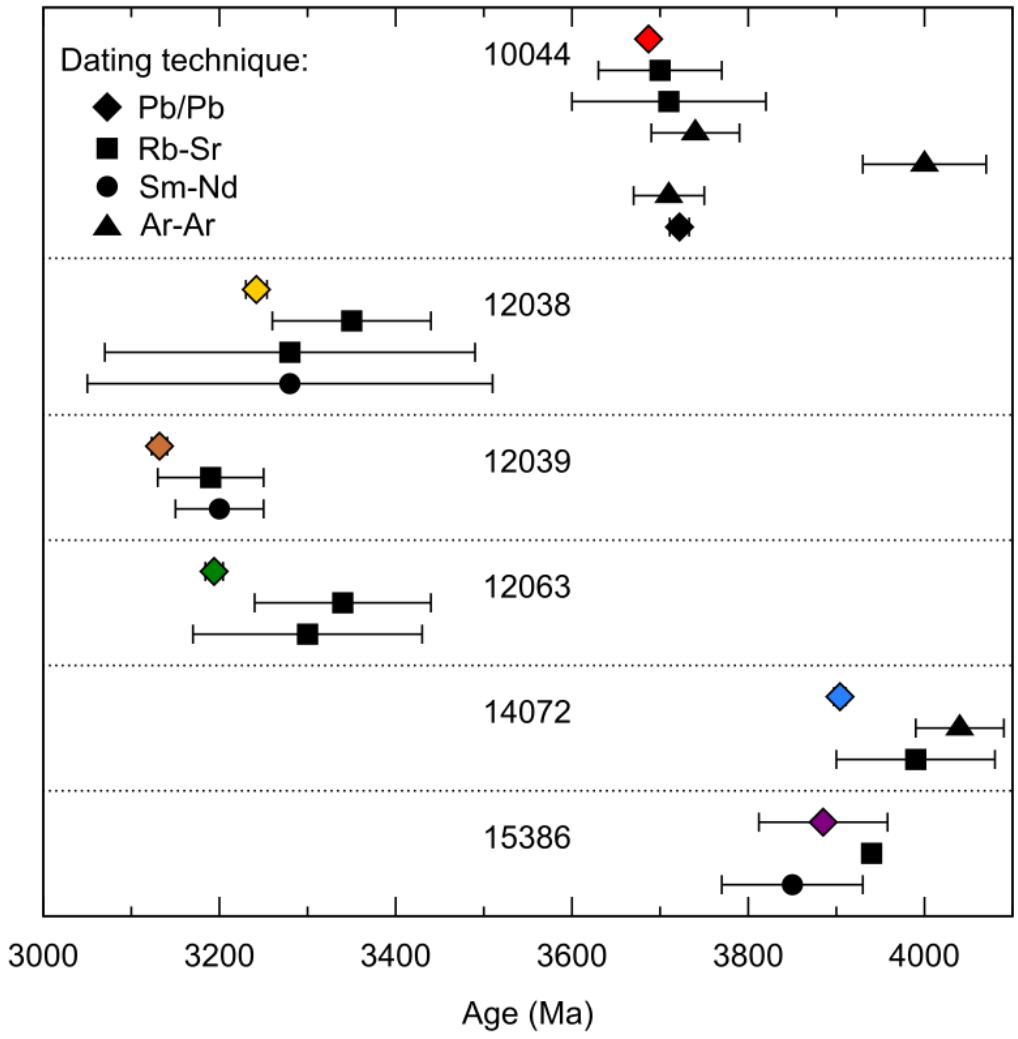

669

670 Figure 5

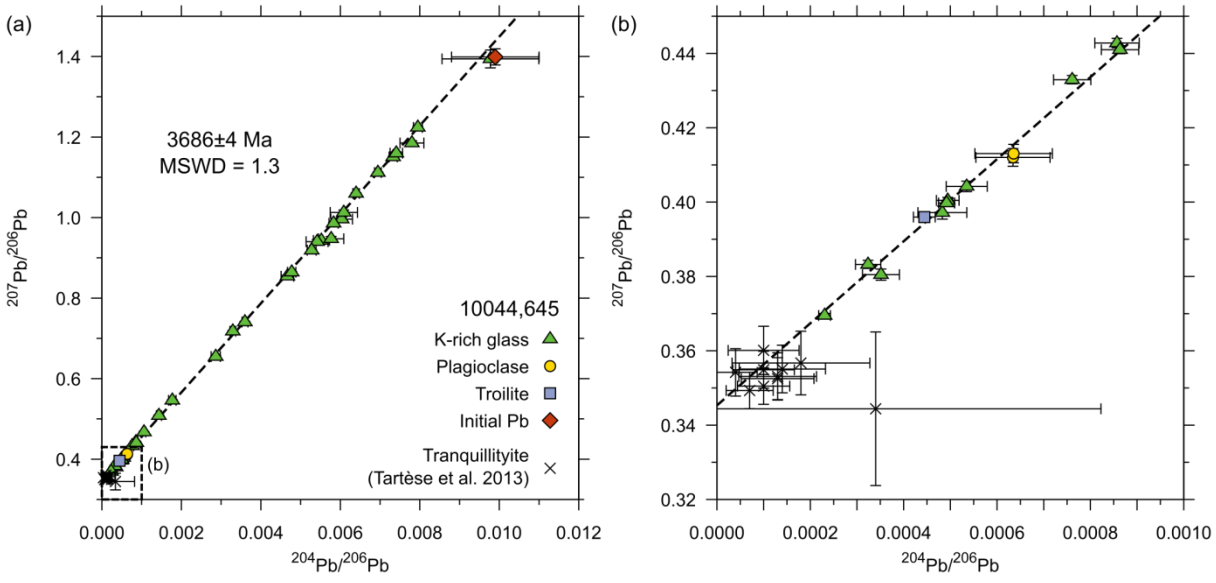

671
672 Figure 6

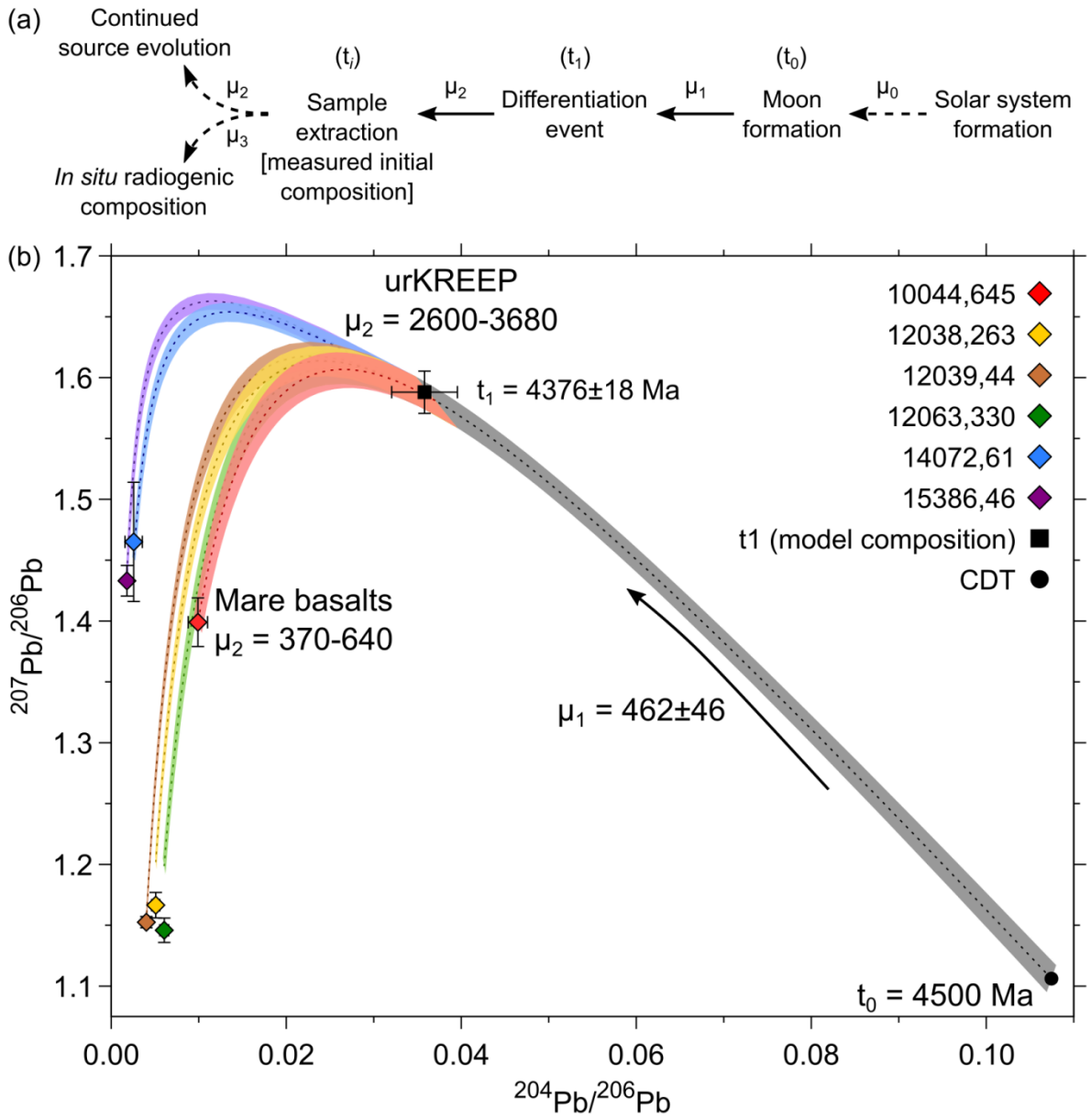

673
674 Figure 7
675

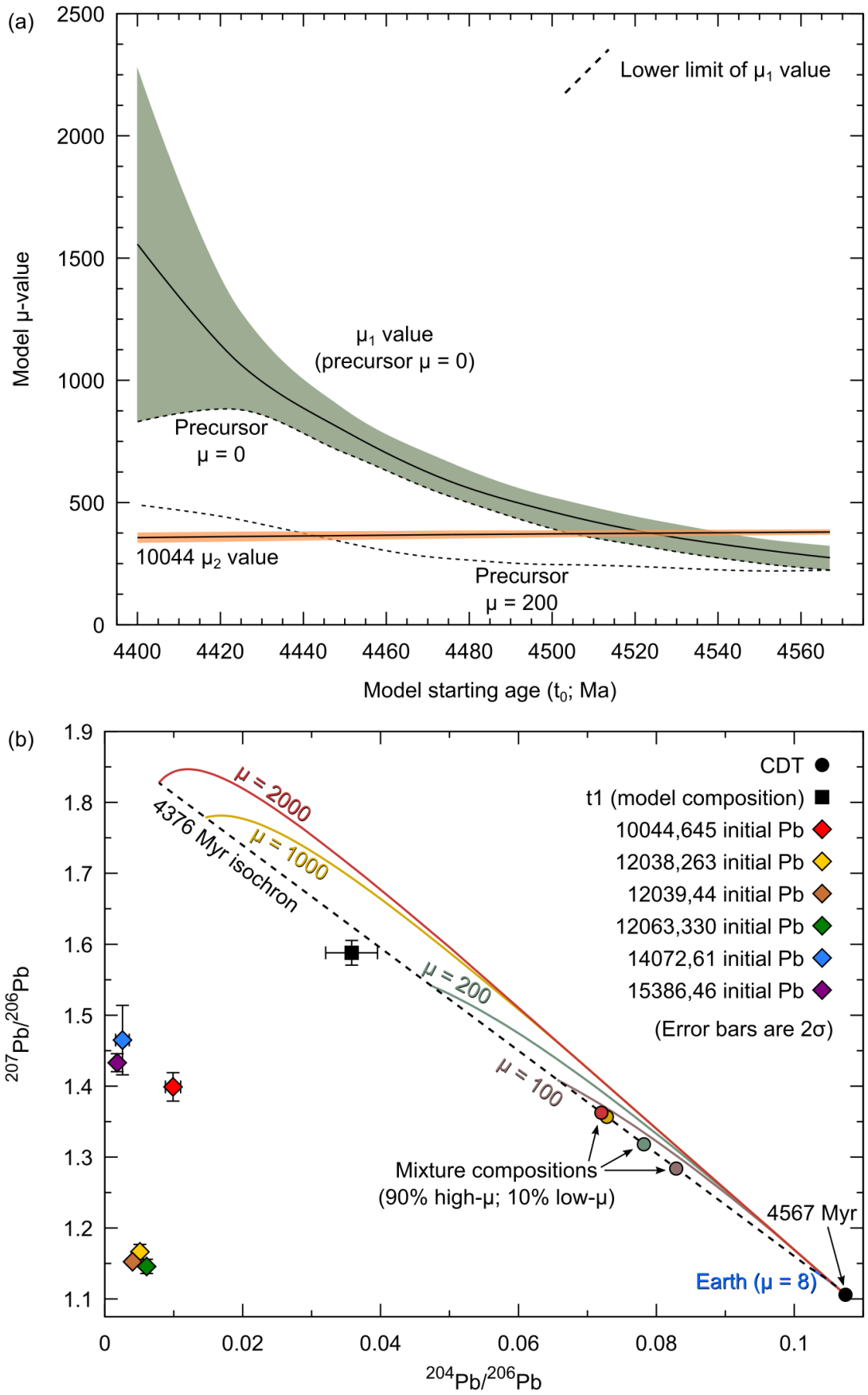

676
677 Figure 8

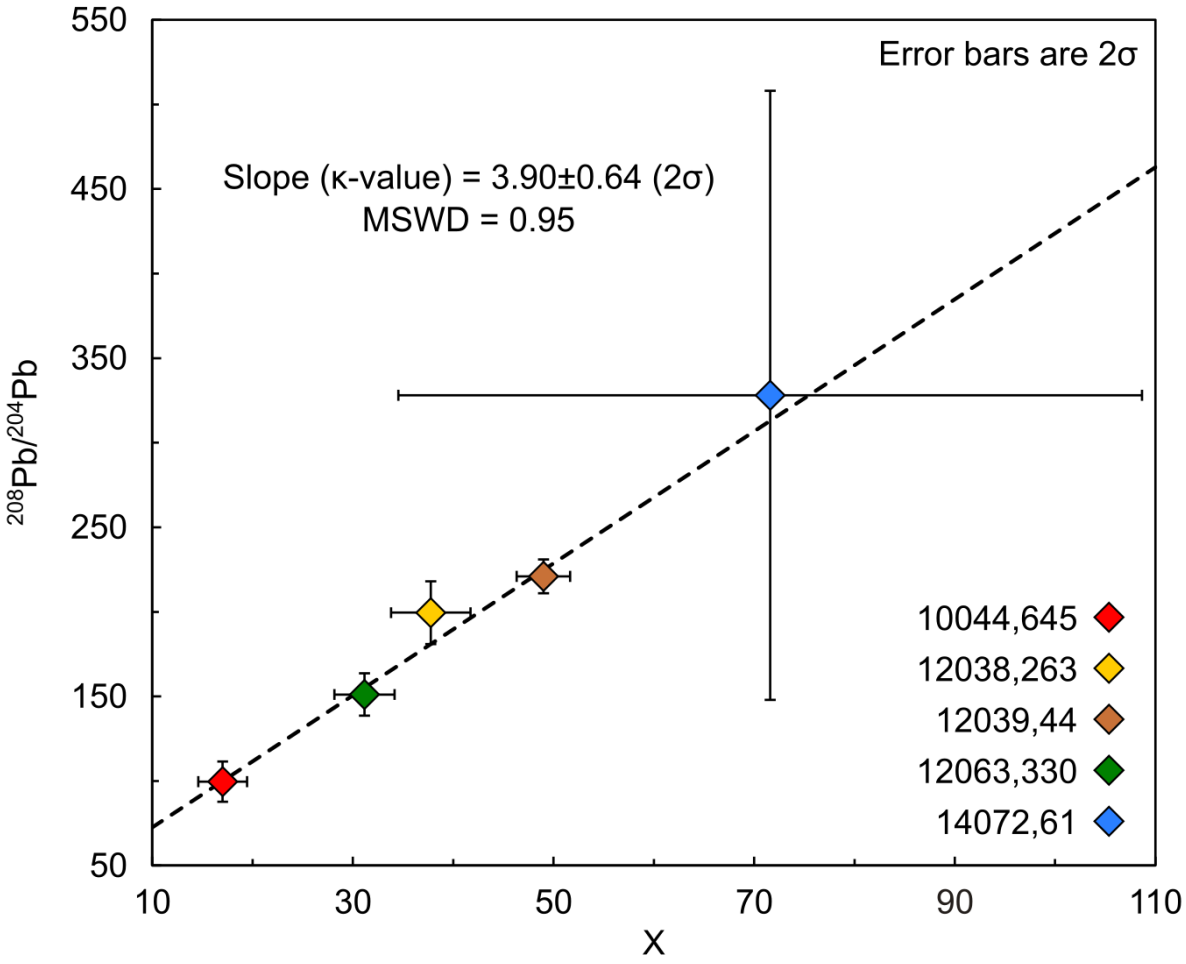

678

679 Figure 9

680